https://doi.org/10.5194/esurf-2020-21
Preprint. Discussion started: 16 April 2020

Earth Surface Dynamics Discussions

Holocene sea-level change on the west coast Bohai Bay, China

Fu Wang[1,2], Yongqiang Zong[3], Barbara Mauz[4,5], Jianfen Li[1,2], Jing Fang[6], Lizhu Tian[1,2], Yongsheng Chen[1,2], Zhiwen Shang[1,2], Xingyu Jiang[1,2], Giorgio Spada[7] and Daniele Melini[8]

[1]Tianjin Center of Geological Survey, China Geological Survey (CGS), Tianjin, China
[2]Key Laboratory of Coast Geo-Environment, China Geological Survey, CGS, Tianjin, China
[3]Department of Earth Sciences, The University of Hong Kong, Hong Kong SAR, China
[4]School of Environmental Sciences, University of Liverpool, Liverpool, UK
[5]Department of Geography and Geology, University of Salzburg, Salzburg, Austria
[6]College of Urban and Environmental Science, Tianjin Normal University, Tianjin, China
[7]Department of Science, University of Urbino, Urbino, Italy
[8]Istituto Nazionale di Geofisica e Vulcanologia, Roma, Italy

Correspondence to to: Fu Wang (wfu@cgs.cn)

Abstract. To constrain models on global sea-level change regional proxy data on coastal change are indispensable. Here, we reconstruct the Holocene sea-level history of the northernmost East China Sea shelf. This region is of great interest owing to its apparent far-field position during the late Quaternary, its broad shelf and its enormous sediment load supplied by the Yellow River. This study collected 15 sediment cores from the coastal plain of west Bohai Bay and extracted 25 sea-level index points through the analyses of sedimentary facies, foraminiferal assemblages and radiocarbon dating. These proxy data indicate a phase of rapid rise from c. -17 m to -4 m of mean sea level between c. 10 ka and 6.5 ka. This was followed by a phase of slow rise from 6.5 ka to 2 ka. In contrast to previous studies our data suggest that the sea level remained c. 2.5 - 1 m below the modern mean sea level during the mid-late Holocene. The difference between proxy data and sea-level predictions based on three GIA models suggests that the Bohai coastal plain experiences subsidence at a rate of around 1.25 mm/a since about 7 ka which masks the mid-Holocene highstand recorded elsewhere in the region. Thus, during the early Holocene rapid rise the sea flooded the coastal plain and the shoreline retreated landwards at a rate of c. 40 m/a. It stayed at the landward maximum marine limit during the mid Holocene when the sea-level rise slowed down allowing vertical sedimentary accretion to occur in the landward areas.

https://doi.org/10.5194/esurf-2020-21
Preprint. Discussion started: 16 April 2020

During the late Holocene fluvial sediment supply outpaced the sea-level change and the shoreline prograded seawards at a rate between 20 and 10 m/a.

KEYWORDS: Sea level; Holocene; Glacial Isostatic Adjustment; Ice Equivalent Sea Level; Bohai Bay

1. Introduction

The sea-level rise since the mid-19th century is one of the major challenges to humanity of the 21st century (IPCC, 2014). The driving mechanisms of this rise are relatively well-known on a global scale, but on a regional scale the mechanisms are modified by local parameters. One of these parameters is the regional Holocene sea-level history, which is a background sea-level signal of variable amplitude. In fact, the regional response to sea-level changes may be very different from the global signal (Nicholls and Cazenave, 2010) and, understanding regional costal environment is a rising demand of policy makers. Here, we study the Holocene sea-level history of Bohai Sea, which is the northernmost part of the Yellow Sea. The area is of special interest because its shoreline is situated on the broad shelf of the East China Sea in the far-field of the former ice sheets. While the far-field position should allow approximating the ice-equivalent sea level, the broad shelf is thought to affect the sea-level (Peltier and Dummond, 2002) by up to 10 m (e.g. Milne and Mitrovica, 2008) in a spatially complex manner. In addition, the exceptionally high supply of fine-grained fluvial sediment to the bay should have influenced shoreline migration in the past. In order to reliably constrain the sea level history in such complex settings, high-resolution proxy data are required and compared with glacio-isostatic adjustment (GIA) model predictions where the difference between model and proxy datum should allow inferring the non-GIA, hence local, impact on the sea-level history. Our study builds on earlier work on late Quaternary stratigraphy and coastal evolution (*e.g.* Cang *et al.*, 1979; Geng, 1981; Wang *et al.*, 1981; Wang, 1982; Yang and Chen, 1985; Zhang *et al.*, 1989; Zhao *et al.*, 1978; Fig. 1) and on published sea-level index points (SLIP) using chenier ridges (Su et al., 2011) and oyster reef (Wang et al., 2011) as sea-level indicators. Li et al. (2015) draw a sea-level band for the west Bohai Bay based on 136 SLIPs and limiting points (LPs). However, misfits between model outputs and observational data are

https://doi.org/10.5194/esurf-2020-21
Preprint. Discussion started: 16 April 2020

apparent (e.g. Wang et al., 2012; Bradley et al., 2016; Li et al., 2015), which are likely caused by the poor quality of the mid-late Holocene sea-level data and insufficient data for the early-mid Holocene.

2. The study area

The study area lies in a mid-latitude, temperate climate zone (Fig. 1a) on the northwestern coast of the East China Sea's wide shelf. Geologically, the Bohai Bay is a depression filled by several kilometer-thick Cenozoic sediment sequences with the top 500 m ascribed to the Quaternary (Wang and Li, 1983). The long-term tectonic subsidence has been estimated to about 1.3-2.0 mm/a at Tianjin City (Wang et al., 2003). The Bay is a semi-enclosed marine environment, connected to the Pacific through a gap between the two peninsulas, Liaodong Peninsulas and Shangdong Peninsulas and the Yellow Sea (Fig. 1b). Our study area is the central coast of the Bay which lies between two deltaic plains, the Yellow River delta in the south and the Luan River delta in the north (Fig. 1b). Several small rivers (e.g. Haihe and Duliujianhe, Fig. 1c) cut through the coastal plain and enter the Bay. The coastal lowland is characterised not only by its low-lying nature, (less than 10 m above sea level), but also by a series of Chenier ridges situated south of the Haihe River and buried oyster reefs situated north of the Haihe River (Fig. 1c). Local reference tidal levels such as mean high waters (MHW) and highest high waters (HHW) are 1.25 m and 2.30 m respectively, based on the four tidal stations on the west coast of Bohai Bay (Fig. 1c). During the Last Glacial Maximum the shoreline moved to the shelf break of the Yellow Sea, more than 1000 km to the east and southeast of our study area (e.g. He, 2006). During the Holocene the sea inundated the coastal area with the shoreline moving about 80 km inland (e.g. Wang et al., 2015). Over 130 SLIPs established for the past 6000 calendar years (e.g. Li et al., 2015) from the oyster reefs and chenier ridges fall into a band between 2.5 m and -2.5 m elevation.

3. Methods

3.1 Sampling and elevation measurements

To obtain sedimentary sequences for this study, we consulted previous studies (*e.g.* Cang *et al.*, 1979; Geng, 1981; Wang *et al.*, 1981; Wang, 1982; Yang and Chen, 1985; Zhang *et al.*, 1989; Zhao *et al.*, 1978; Xue et al., 1993) to learn where in the bay marine deposits are dominant and where the landward limit of the last marine transgression should occur. We then collected 15 cores along W-E transects from the modern shoreline to 80 km inland (Fig. 1c), using a rotary drilling corer. Transect A, comprising 6 cores, stretches from the modern shoreline 80 km inland and crosses the inferred Holocene transgression limit (Xue, 1993). Transects B, C and D, comprising 9 cores, cross the transgression limit a little further south (Fig. 1c). The surface elevations of the drilled cores were leveled to the National Yellow Sea 85 datum (or mean sea level, MSL) using a GPS-RTK system with a precision of 3 cm. The GPS-RTK raw data were corrected and processed to National Yellow Sea 85 datum system by the CORS system network available from the Hebei Institute of Surveying and Mapping with National measurement qualification.

3.2 Sediment and peat analyses

In the laboratory, the sediment cores were opened, photographed and recorded for sedimentary characteristics including grain size, color, physical sedimentary structures, and content of organic material. To study the degree of marine influence in the muddy sediment sequences, sub-samples were collected in 20 cm intervals. These were analysed with respect to diatoms and foraminifera with a subsequent focus on the foraminifera due to poor preservation of diatoms. The foraminifera of the >63μm fraction of 20 g dry sample were counted (e.g., Wang et al., 1985) following studies on modern foraminifera (e.g. Li, 1985; Li et al., 2009). Sediment description followed Shennan et al. (2015): where in the sediment sequences foraminifera first appear and/or significantly increase (from zero or less than 10 to more than 50) is noted as transgressive contact, while the sediment horizon where foraminifera disappear and/or decrease significantly are noted as regressive contact. These changes are often associated with lithological changes, such as from salt-marsh peaty sediment to estuarine sandy sediment or tidal muddy sediment across a transgressive contact, or vice

https://doi.org/10.5194/esurf-2020-21
Preprint. Discussion started: 16 April 2020

Earth Surface Dynamics Discussions Open Access EGU

versa. In addition, peat material was analysed in terms of its foraminifera content so that salt-marsh peat can be differentiated from freshwater peat.

3.3 Analysis of compaction

Because the Holocene marine deposits are mainly unconsolidated clayey silt with around 0.74% organic matter (Wang et al. 2015) post-depositional auto-compaction (Brain et al., 2015) may have led to lowering of the SLIP. According to Feng et al. (1999), the water content and compaction of marine sediments show positive correlation with the down-core reduction of water content of the Holocene marine sediment being about 10%. Based on these observations, we assumed the maximum lowering is about 10% of the total thickness of the compressible sediment beneath each SLIP. Consequently, the total lowering for an affected SLIP is 10% of the total thickness of the compressible sequence beneath the dated layer divided by the post-depositional lapse time proportional to the past 9000 years (e.g. Xiong et al., 2018), i.e. since the marine transgression in the study area.

3.4 Radiocarbon analyses

69 bulk organic sediment samples and corresponding peat or plant subsamples from salt-marsh peat were chosen for AMS radiocarbon analysis because these can give more reliable ages for the SLIPs. The resulting radiocarbon ages were converted to conventional ages after isotopic fractionation were corrected based on $\delta^{13}C$ results. The conventional radiocarbon ages were calibrated to calendar years using the data set Intcal13 of Calib Rev 7.0.2 for organic samples, peat and plant samples (Reimer, *et al*., 2013). Because Shang et al. (2018) reported age overestimation of 467 years for the bulk organic fraction of salt-marsh peaty clay compared to the corresponding peat fraction, all the AMS ^{14}C ages between 4000 to 9000 BP obtained from salt-marsh samples were corrected by $Y=0.99X-466.5$ (Y is the corrected age, X is the age obtained from the organic fractions; Shang et al., 2018) except one <600 years age from borehole Q7 (Table 1).

https://doi.org/10.5194/esurf-2020-21
Preprint. Discussion started: 16 April 2020

3.5 Sea-level index points (SLIPs)

For determining SLIPs salt-marsh peaty clay layers were used. To convert the dated peat layers into a SLIP, the modern analogue approach was used by measuring the elevation of the modern open tidal flat (Fig. 2) and sampling its surface for their foraminiferal content. Following the studies of the modern foraminifera assemblage (Li, 2009) *Ammonia beccarii* typically occurs in the upper part of an intertidal zone and *Elphidium simplex* in the lower intertidal zone. The elevation data of the modern analogue samples for which the foraminifera assemblage confirmed the salt-marsh origin of the peat (i.e. dominance of *Ammonia beccarii*) were then used to infer the indicative meaning of the dated peat layer: the palaeo-mean sea level is the midpoint between high water of spring tides (HHW:+2.3 m) and mean high waters (MHW:+1.25 m) which is 1.78 m with ±0.53 m uncertainty (Wang et al., 2002, 2003; Li et al., 2015). For each dated salt-marsh peat layer the indicative meaning and range, the total amount of possible lowering in elevation due to sediment compaction and the reconstructed elevation of palaeo-MSL are listed in Table 1.

3.6 GIA modelling

The time-evolution of sea level was obtained using the open source program SELEN (Spada and Stocchi, 2007) to solve the "Sea Level Equation" (SLE) in the standard form proposed in the seminal work of Farrell and Clark (1976). In its most recent development, SELEN (version 4) solves a generalized SLE that accounts for the horizontal migration of the shoreline in response to sea-level rise, for the transition from grounded to floating ice and for Earth's rotational feedback on sea level (Spada and Melini, 2019). The programme combines the two basic elements of GIA modelling (Earth's rheological profile and ice melting history since the Last Glacial Maximum) assuming a Maxwell viscoelastic incompressible rheology. The GIA models adopted are ICE-5G(VM2) (Peltier et al., 2004), ICE-6G(VM5a) (Peltier et al., 2012), both available on the home page of WR Peltier, and the one developed by Kurt Lambeck and colleagues (National Australian University, denoted as ANU hereafter; Nakada and Lambeck, 1987, Lambeck et al., 2003) provided to us by A Purcell (pers. com. 2016). Intrinsic uncertainties are estimated from the comparison of GIA predictions obtained with the models listed above (Melini and Spada, 2019). Table S1 summarises the values used for

https://doi.org/10.5194/esurf-2020-21
Preprint. Discussion started: 16 April 2020

each model. The paleo-topography has been solved iteratively, using the present-day global relief given by model ETOPO1 (Amante and Eakins, 2009). All the fields have been expanded to harmonic degree 512, on an equal-area icosahedron-based grid (Tegmark, 1996) with a uniform resolution of ~20 km. The rotational effect on sea-level change has been taken into account by adopting the "revised rotational theory" (Wahr and Mitrovica, 2011).

4. Results

Lithostratigraphically, the cores show a succession of terrigenous (including fresh-water swamp, river channel, flood plain), salt-marsh and marine sediments (Table S2) with a clear W-E trend from terrestrial to marine dominance of deposits (Fig. 3-6). The around 80 km long transect A shows this trend: close to the modern shoreline pre-Holocene terrigenous sediments are overlain by basal peat including salt-marsh peat or peaty clay. Further inland these are replaced by fresh-water peat overlain by salt marsh and intertidal sediments and, above, by terrigenous sediments. The cores DC01, CZ01 and CZ02 are composed of fluvial sediments only, roughly confirming the Holocene maximum transgression inferred by Xue (1993). Multiple shifts between salt marsh, marine and fluvial deposits are noticeable in cores QX02, QX03, CZ61 which originate from the central part of the study area.

Marsh deposits are either a blackish and thin freshwater peat mostly interbedded in yellowish fluvial sediments or a yellowish-brown salt-marsh peat bearing intertidal foraminifera (Table 1). Their lower boundaries are usually sharp, and their upper boundaries are mostly diffused or the salt-marsh peat changes gradually into dark grey intertidal sediments. Salt-marsh peat is intercalated in marine sediment sequences (i.e. QX01, QX02, CZ61, CZ85, CZ66 and CZ03, Fig. 3-6), particularly at sites that are close to the Holocene maximum landward limit.

In the core deposits we found *Ammonia beccarii, Quinqueloculina akneriana rotunda, Protelphidium tuberculatum*. The foraminifera assemblages of the lower part of the intertidal zone and the near-shore shallow sea area are similar. The abundance is either biased towards *Ammonia beccarii* or it is relatively small. The latter is most probably due to the area being situated above the MHW and, hence, subject to

https://doi.org/10.5194/esurf-2020-21
Preprint. Discussion started: 16 April 2020

evaporation during low tide, with the consequence of a relatively high and highly variable salt content of the pore water in the intertidal zone. The bias towards salt-tolerant species is confirmed by the modern analogue samples (Fig. 2, Table 1).

The age of the basal peat ranges between 10047 cal BP and 7829 cal BP (Table 1). The spatial distribution of the ages confirms the E-W trend of the Holocene transgression where the oldest age is close to the modern shoreline and the youngest age is close to the maximum transgression limit.

4.1 Indicative meaning and range

The data obtained from the modern analogue shows that the tidal flat can be divided into two sub-environments: intertidal with bioturbation (worm hole developed to tidal surface) and supratidal with salt-marsh vegetation (Fig. 2). Within the supratidal and salt-marsh zones, the foraminiferal assemblages are dominated by *Ammonia beccarii* and other intertidal species (Fig. 5) covering an elevational range from +1.42 m to +2.00 m above msl, including the +1.79m boundary of salt marsh with plants. At sites below these elevations, i.e. intertidal with bioturbation (Fig. 2), the foraminiferal assemblages are dominated by *Elphidium simplex, Ammonia beccarii and Pseudogyroidina Sinensis*. This foraminiferal zone covers an elevational range from 1.42 m to the present MSL. Our results from the core sediments show that the foraminiferal assemblages are mostly dominated by *Ammonia beccarii*.

4.2 Sea-level Index points

In total 25 sea-level index points were established from the dated basal salt-marsh peat using the information obtained from the modern analogue. In Core Q7, at the most seaward location in the study area, the basal SLIP is dated to ~9700 cal BP (Table 1), marking the onset of marine inundation of the study area. The overlying marine sequence is capped by a thick layer of shelly gravels at 1.30 m depth and the associated SLIP is dated to 540 cal BP. This marks the upper end of the marine sequence as foraminifera start to disappear alongside a change from intertidal to supratidal environmental conditions. The cores ZW15, QX02, QX03, QX01 show the same sequence as Q7 and provide 6 SLIPs. 19 SLIPs were collected from other cores (Table 1).

https://doi.org/10.5194/esurf-2020-21
Preprint. Discussion started: 16 April 2020

4.3 Observed and predicted sea level

Figure 7a compares observational data and sea-level predictions generated in this study. It shows that none of GIA models approximates the observations. The difference ranges between around 14 m at 9 ka and 3 m at 2.5 ka. While SLIP data suggest a rising rate of ~0.4 cm/a during the early Holocene, the GIA models indicate ~0.5 cm/a (ICE-X) and ~0.9 cm/a (ANU). For the mid-late Holocene SLIP data suggest ~0.04 cm/a rising rate while the GIA models indicate a falling sea level. Predictions obtained from ICE-5G and ICE-6G are relatively similar but deviate from each other in the timing of the mid-Holocene sea-level highstand. All three GIA models predict a mid-Holocene sea-level highstand (4.6 m -3.4 m) at 7-6 ka while the SLIP data remain below modern sea level until 2 ka.

5. Discussion

5.1 Quality of SLIP data

Owing to elevated salinity of the coastal water samples from both cores and modern tidal flat are characterised by low microfauna diversity and low number of foraminifera species. This precludes the use of transfer function statistics and compels analysis based on direct comparison with the modern environment. We have solved this analytical problem by establishing SLIPs exclusively from basal salt-marsh peats in transgressive contact and corrected for compaction. With a general uncertainty of around 1.1 m our new SLIPs are therefore more precise than previously published data (Li et al., 2015) mostly obtained from chenier ridges, oyster reefs and marine shells. Notwithstanding SLIP improvement in terms of accuracy and precision, fluctuation of the data exist that can exceed 1 m (e.g. at 3.9 ka and at 5.2 ka, Fig. 7). Although hard to prove due to lack of data, we believe that these fluctuations are caused by groundwater extraction which lowers the surface in places.

5.2 The observed Holocene sea-level rise

The SLIPs established indicate two phases of sea-level rise during the Holocene. The first phase occurred in the early Holocene until ~6.5 ka when the sea level rose from -17 m to -4 m. The second phase occurred from

~6.5 ka to 2 ka when the sea level rose from -4 m to -2 m. The oldest Holocene shoreline in Bohai Bay, situated at -17.2 m and dated to 9700 cal BP, is associated with a transgressive systems tract (Tian et al., 2017), the water depth of which suggests ~-20 m at 9400 cal BP as the start of the transgression. The discrepancy is caused by sea ingression occurring ~300 years before Bohai Bay shelf experienced inundation as indicated by a paleo-river channel deposit (Fig. 2) underlying the Holocene basal peat in core Q7. We take it therefore for certain that the sea level reached around -15 m at ~9 ka. The final phase from 2 ka to today is constrained by only one SLLP from core Q7 dated to 540 cal BP at ~0.5 m (Table 1). Lithostratigraphic data (Shang et al., 2016) suggest that surface of the intertidal sediment body remained very close to zero m from the landward limit of the marine transgression to about 2 km inland from the present shoreline. Further inland, in borehole ZW15 the surface elevation of the same intertidal sediment body is ~3.0 m lower than in core Q7 (Fig. 3, 4) suggesting a rise of sea level in Bohai Bay in the last 1000 years.

5.3 Observed and predicted Holocene sea level

We compare our observational data with GIA models employed in this study and with Bradley et al. (2016; henceforth denoted as BRAD; see also Table S1) who examined several ice-melting scenarios together with a range of Earth-model parameters, and validated model outputs using published SLIP data from East China Sea coast including Bohai Bay.

The comparison shows a significant discrepancy for all GIA models (Fig. 7a) including BRAD with differences ranging between around 14 m in the early-mid Holocene and 3 m in the late Holocene. While the ICE-X models approximate the observed early Holocene rising rate, the timing of this rise is offset by about 2000 years. In the ANU model the early Holocene sea level rises almost twice as fast as the observed one with an offset of ~500 years. Thus, the observed sea level rises slower than the modelled sea level. Because the misfit almost disappears south of Bohai Bay (Fig. S1), the most obvious explanation is subsidence of the coastal plain. Subsidence is a non-GIA component and should become evident through the residuals (i.e. the difference between observation and prediction per unit of time; Fig. 7b). Indeed, we identify linearity of residuals for the period 7-0 ka, suggesting that subsidence dominates the local sea-level signal after the rise of the eustatic sea level has slowed down. A subsidence rate of 1.25 mm/a is estimated from the residuals, similar to Wang et al. (2003) who deduced a rate of ~1.5 mm/a from the 400-500 m thick Quaternary sequence in the bay. It is possible that fluvial sediment supply enhanced the subsidence rate in the Holocene. The Yellow River's annual discharge into Bohai Bay is estimated to 0.2 Gt until 740AD rising to 1.2 Gt until around 1800 when widespread farming on the loess plateau started increasing the river's sediment load (Best, 2019). Thus, the sea-level rise in Bohai Bay is in the early Holocene dominated by the global sea-level rise and associated GIA effects, while in the mid-late Holocene it is dominated by a combination of tectonic subsidence and fluvial sediment load.

6. Conclusions

Using advanced methods for field survey and identification of sea-level markers, we have established new precise sea-level index points for the northernmost embayment of the Yellow Sea. Our new data are not only different to previously published data in that they do not show the expected mid-Holocene sea level highstand, but also different to global GIA models. We see that as soon as ice melting has ceased, local processes control shoreline migration and coast evolution. This indicates that more emphasis should be placed on regional coast and sea-level change modelling under a global sea-level rising future as the local government need more specific and effective advice to deal with coastal flooding.

7. ACKNOWLEDGMENTS

We thank anonymous reviewers, who gave many constructive suggestions, and this work was supported by the the China Geological Survey, CGS (DD20189506) and National Natural Science Foundation of China (Grant no. 41476074, 41806109, 41972196). We also thank Mr. Pei Y. and Shang Z., who contributed to fieldwork and sample preparation respectively.

References

Amante, C. and Eakins, B.: ETOPO1 Arc-Minute Global Relief Model: Procedures, Data Source and Analysis. Tech. rep, DOI: 10.7289/V5C8276M, 2009.

Bard, E., Hamelin, B., Arnold, M., Montaggioni, L., Cabioch, G., Faure, G., Rougerie, F.: Deglacial sea-level record from Tahiti corals and the timing of global meltwater discharge. Nature, 382, 241–244. https://doi.org/10.1038/382241a0, 1996.

Bard, E., Hamelin, B. and Delanghe-Sabatier, D.: Deglacial meltwater pulse 1B and Younger Dryas sea levels revisited with boreholes at Tahiti. Science, 327, 1235-1237. DOI: 10.1126/science.1180557, 2010.

Bradley, S.L., Milne, G.A., Horton, B.P., Zong, Y.Q.: Modelling sea level data from China and Malay-Thailand to estimate Holocene ice-volume equivalent sea level change. Quaternary Science Reviews, 137, 54–68. DOI: 10.1016/j.quascirev.2016.02.002, 2016.

Brain, M.J., Kemp, A.C., Horton, B.P., Culver, S.J., Parnell, A.C., Cahill, N.: Quantifying the contribution of sediment compaction to late Holocene salt-marsh sea-level reconstructions, North Carolina, USA. Quaternary Research, 83, 41-51. DOI: 10.1016/j.yqres.2014.08.003, 2015.

Brain, M.J. Chapter 30 Compaction. In: Shennan, I., Long, A.J., Horton, B.P. (Eds.): Handbook of Sea-level Research. John Wiley & Sons Ltd. Chichester, UK, 2015.

Cang, S.X., Zhao, S.L., Zhang, H.C., Huang, Q.F.: Middle Pleistocene paleoecology, paleoclimatology and paleogeography of the western coast of Bohai Gulf. Acta Palaeontologica Sinica 18(6): 579–591. DOI： 10.19800/j.cnki.aps.1979.06.006, 1979 (in Chinese with English abstract).

Cronin, T.M.: Rapid sea-level rise. Quaternary Science Review, 56, 11-30. https://doi.org/10.1016/j.quascirev.2012.08.021, 2012.

Engelhart, S. E., Peltier, W. R., Horton, B. P., Khan, N. S., Liu, S., Vacchi, M.: A Holocene Database of Relative Sea Levels for North America and the Caribbean: Implications for Geophysical Models. American Geophysical Union, Fall Meeting 2011, abstract #GC43D–0964, 2011

Farrell, W. and Clark, J.: On postglacial sea-level. Geophys. J. Roy. Astr. S., 46, 647–667. DOI: 10.1111/j.1365-246X.1976.tb01252.x, 1976

https://doi.org/10.5194/esurf-2020-21
Preprint. Discussion started: 16 April 2020

Feng, X.L., Lin, L., Zhuang, Z.Y, Pan, S.C.: The relationship between geotechnical paramenters and sedimentary environment of soil layers since Holocene in modern Huanghe subaqueous Delta. Coastal Engineering, 18, 4, 1-7. DOI: CNKI:SUN:HAGC.0.1999-04-000, 1999 (in Chinese with English abstract).

Funabiki, A., Haruyama, S., Nguyen, V.Q., Pham, V.H., Dinh, H.T.: Holocene delta plain development in the Song Hong (Red River) delta, Vietnam. Journal of Asian Earth Sciences, 30, 518−529. DOI: 10.1016/j.jseaes.2006.11.013, 2007.

Geng, X.S.: Marine transgressions and regressions in east China since late Pleistocene Epoch. Acta Oceanlogica Sinica, 3(1), 114−130. http://www.hyxb.org.cn/aos/ch/reader/create_pdf.aspx?file_no=19810110&flag=&journal_id=aos&year_id=1981, 1981 (in Chinese with English abstract).

Geyh, M.A., Kudrass, H.R.and Streif, H.: Sea-level changes during the Late Pleistocene and Holocene in the Strait of Malacca. Nature, 278, 441−443. DOI：10.1038/278441a0, 1979.

Hanebuth, T., Stattegger, K.and Grootes, P.M.: Rapid flooding of the Sunda Shelf: a late-glacial sea-level record. Science, 288, 1033-1035. DOI: 10.1126/science.288.5468.1033, 2000.

He, Q.X.(Eds.): Marine Sedimentary Geology of China. Beijing: China Ocean Press: 464−466, 2006 (in Chinese).

Hori, K., Saito, Y., Zhao, Q., Cheng, X., Wang, P., Sato, Y., Li, C., 2001. Sedimentary facies and Holocene progradation rates of the Changjiang (Yangtze) delta, China. Geomorphology, 41, 233−248. DOI: 10.1016/S0169-555X(01)00119-2, 2001.

Hori, K., Tanabe, S., Saito, Y., Haruyama, S., Nguyen, V., Kitamura, A.: Delta initiation and Holocene sea-level change: Example from the Song Hong (Red River) Delta, Vietnam. Sedimentary Geology, 164, 237−249. DOI: 10.1016/j.sedgeo.2003.10.008, 2004.

Hori, K. and Saito, Y.: An early Holocene sea-level jump and delta initiation. Geophysical Research Letters, 34, L18401. DOI: 10.1029/2007gl031029, 2007.

https://doi.org/10.5194/esurf-2020-21
Preprint. Discussion started: 16 April 2020

Earth Surface Dynamics
Discussions

Horton, B. P., Gibbard, P. L., Milne, G. M., Morley, R. J., Purintavaragul, C., Stargardt, J. M.: Holocene sea levels and palaeoenvironments, Malay-Thai Peninsula, Southeast Asia. Holocene, 15(8), 1199−1213. https://doi.org/10.1191/0959683605hl891rp, 2005.

IPCC: Climate Change 2014: Synthesis Report Summary for Policymakers, 1-31, 2014.

Lambeck, K., Woodroffe, C.D., Antonioli, F., Anzidei, M., Gehrels, W.R., Laborel, J., Wright, A.J.: Paleoenvironmental records, geophysical modeling, and reconstruction of sea-level trends and variability on centennial and longer timescales, In: Understanding Sea-Level Rise and Variability (Church, J. A.; Woodroffe, P.L.; Aarup, T.; Wilson, W.S., eds.), Wiley-Blackwell, 61−121. DOI: 10.1002/9781444323276.ch4, 2010.

Lambeck, K., Rouby, H., Purcell, A., Sun, Y., Sambridge, M.: Sea level and global ice volumes from the Last Glacial Maximum to the Holocene. Proceedings of the National Academy of Sciences, 111, 15296−15303. DOI: 10.1073/pnas.1411762111, 2014.

Lambeck, K., Purcell, A., Johnston, P., Nakada, M., Yokoyama, Y.: Water-load definition in the glacio-hydro-isostatic sea-level equation. Quaternary Science Reviews, 137, 54-68. DOI: 10.1016/s0277-3791(02)00142-7, 2003.

Li, S.Y.: Preliminary investigation of the ancient shorelines and buried cultural relics along the west Bohai Bay. Archaeology, 652−657. DOI: CNKI:SUN:KAGU.0.1962-12-006 (in Chinese).

Li, C., Chen, Q., Zhang, J., Yang, S, Fan, D.: Stratigraphy and paleoenvironmental changes in the Yangtze delta during the Late Quaternary. Journal of Asian Earth Sciences, 18, 453−469. DOI: 10.1016/S1367-9120(99)00078-4, 2000.

Li, J., Pei, Y., Wang, F., Wang, H.: Distribution and environmental significance of living foraminiferal assemblages and taphocoenose in Tianjin intertidal zone, the west coast of Bohai Bay. Marine geology & Quaternary geology, 29(3), 9−21. DOI: CNKI:SUN:HYDZ.0.2009-03-004, 2009. (in Chinese with English abstract).

https://doi.org/10.5194/esurf-2020-21
Preprint. Discussion started: 16 April 2020

Li, J., Shang, Z., Wang, F., Chen, Y., Tian, L., Jiang, X., Wang, H.: Holocene sea level change on the west coast of the Bohai Bay. Quaternary Sciences, 35(2), 243−264. DOI: 10.11928/j.issn.1001-7410.2015.02.01, 2015 (in Chinese with English abstract).

Li, J.F., Shang, Z.W., Jiang, X.Y., Chen, Y.S., Wang F., Tian, L.Z., Wang, H., 2016. Sea-level indicated by foraminifera assemblages living in open muddy flats with or without influence of the Chenier ridges in Bohai Bay coastal area. Geological Bulletin of China 35(10), 1578-1583. DOI: 10.3969/j.issn.1671-2552.2016.10.003, 2016 (in Chinese with English abstract).

Li, S.L.: Distribution of the foraminiferal thanatocoenosis of PEARL River estuary. Marine geology & Quaternary Geology, 5(2), 83−101. DOI：10.16562/j.cnki.0256-1492.1985.02.009, 1985 (in Chinese with English abstract).

LIoyd, J.M., Zong, Y., Fish, P., Innes, J.B.: Holocene and Late glacial relative sea-level change in north-west England: implications for glacial isostatic adjustment models. Journal of Quaternary Science, 28, 59−70. DOI: 10.1002/jqs.2587, 2013.

Melini, D. and Spada, G.: Some remarks on Glacial Isostatic Adjustment modelling uncertainties. Geophysical Journal International, 218, 1, 401–413. https://doi.org/10.1093/gji/ggz158, 2019.

Mitrovica, J. and Wahr, J.: Ice Age Earth Rotation. Annual Review of Earth and Planetary Sciences, 39, 577-616. DOI: 10.1146/annurev-earth-040610-133404, 2011.

Nakada, M. and Lambeck, K.: Glacial rebound and relative sea-level variations: a new appraisal. Geophysical Journal International, 90, 1, 171-224. DOI: 10.1111/j.1365-246X.1987.tb00680.x, 1987.

Nicholls, R.J. and Cazenave A.: Sea-level rise and its impact on coastal zones. Science, 328, 1517-1520. DOI: 10.1126/science.1185782, 2010.

Peltier, W.R.: Global glacial isostasy and the surface of the ice-age Earth: the ICE-5G (VM2) Model and GRACE, Annu. Rev. Earth Pl. Sc., 32, 111–149. https://doi.org/10.1146/annurev.earth.32.082503.144359, 2004.

https://doi.org/10.5194/esurf-2020-21
Preprint. Discussion started: 16 April 2020

Peltier, W.R., Drummond, R., and Roy, K.: Comment on Ocean mass from GRACE and glacial isostatic adjustment by DP Chambers et al., J. Geophys. Res.-Sol. Ea., 117, B11403. https://doi.org/10.1029/2011JB008967, 2012.

Peltier, W.R., Argus, D.F., Drummond, R., Moore, A.W.: Space geodesy constrains ice-age terminal deglaciation: the global ICE-6G C (VM5a) model. Journal of Geophysical Research: Solid Earth, 120, 450–487. https://doi.org/10.1002/2014JB011176, 2015.

Reimer, P.J., Bard, E., Bayliss, A., Beck, J.W., Blackwell, P.G., Ramsey, C.B., Buck, C.E., Cheng, H., Edwards, R.L., Friedrich, M., Grootes, P.M., Guilderson, T.P., Haflidason, H., Hajdas, I., Hatté, C., Heaton, T.J., Hogg, A.G., Hughen, K.A., Kaiser, K.F., Kromer, B., Manning, S.W., Niu, M., Reimer, R.W., Richards, D.A., Scott, E.M., Southon, J.R., Turney, C.S.M., van der Plicht, J.: IntCal13 and MARINE13 radiocarbon age calibration curves 0−50000 years cal BP. Radiocarbon, 55(4), 1869−1887. doi: 10.2458/azu_js_rc.55.16947Bronk Ramsey C and Lee S (2013), 2013.

Shang, Z.W., Wang, F., Li, J.F., Marshall, W.A., Chen, Y.S., Jiang, X.Y., Tian, L.Z., Wang, H.: New residence times of the Holocene reworked shells on the west coast of Bohai Bay, China. Journal of Asian Earth Sciences, 115, 492−506. DOI: 10.1016/j.jseaes.2015.10.008, 2016.

Shang, Z.W., Wang, F., Fang J., Li, J.F., Chen, Y.S., Jiang, X.Y., Tian, L.Z., Wang, H.: Radiocarbon ages of different fractions of peat on coastal lowland of Bohai Bay: marine influence? Journal of Oceanology and Limnology, https://doi.org/10.1007/s00343-019-7091-7, 2018.

Shennan, I., Long, A.J. and Horton, B.P.(Eds.): Handbook of sea-level research. Published by John Wiley & Sons, Ltd., 2015.

Spada, G. and Stocchi, P.: SELEN: a Fortran 90 program for solving the “Sea Level Equation”, Comput. Geosci., 33, 538–562. DOI: 10.1016/j.cageo.2006.08.006, 2007.

Spada, G. and Melini, D.: SELEN4 (SELEN version 4.0): a Fortran program for solving the gravitationally and topographically self-consistent sea-level equation in glacial isostatic adjustment modelling. Geoscientific Model Development, 12, 5055-5075. DOI: 10.5194/gmd-12-5055-2019, 2019

https://doi.org/10.5194/esurf-2020-21
Preprint. Discussion started: 16 April 2020

Su, S.W., Shang, Z.W., Wang, F., Wang, H.: Holocene Chenier: spatial and temporal distribution and sea level indicators in Bohai Bay. Geological Bulletin of China, 30(9), 1382–1395. DOI: 10.1007/s11589-011-0776-4, 2011(in Chinese with English abstract).

Sun, Y.Y., Wu, P., Huang, G.Q., Zong, Y.Q.: Holocene sea-level reconstruction for Guangdong coast and a comparison with GIA model outputs. Quaternary Sciences, 35(2), 282–290. DOI:10.11928/j.issn.1001-7410.2015.02.04, 2015 (in Chinese with English abstract).

Ta, T.K.O., Nguyen, V.L., Taeishi, M., Kobayashi, I., Tanabe, S., Saito, Y.: Holocene delta evolution and sediment discharge of the Mekong River, South Vietnam. Quaternary Science Reviews, 21, 1807–1819. DOI: 10.1016/s0277-3791(02)00007-0, 2002.

Tam, C-Y., Zong, Y., Kamaludin, bH., Hamlee, bI., Habibah, bJ., Xiong, H., Wu, P., Sun, Y., Huang, G., Zheng, Z.: A below-the-present late Holocene relative sea level and the glacial isostatic adjustment during the Holocene in the Malay Peninsula. Quaternary Science Reviews, 201, 206-222. https://doi.org/10.1016/j.quascirev.2018.10.009, 2018.

Tamura, T., Saito, Y., Sieng, S., Ben B., Kong, M., Sim, I., Choup, S., Akiba, F.: Initiation of the Mekong River delta at 8ka: evidence from the sedimentary succession in the Cambodian lowland. Quaternary Science Reviews, 28, 327–344. DOI: 10.1016/j.quascirev.2008.10.010, 2009.

Tanabe, S., Saito, Y., Quang, L.V., Hanebuth, T.J.J., Quang, L.N., Kitamura, A.: Holocene evolution of the Song Hong (Red River) delta system, northern Vietnam. Sedimentary Geology, 187, 29–61. http://377.rm.cglhub.com/10.1016/j.sedgeo.2005.12.004, 2006.

Tegmark, M.: An icosahedron-based method for pixelizing the celestial sphere, Astrophys. J., 470, L81–L85, https://doi.org/10.1086/310310, 1996.

Wang, F., Li, J.F., Chen, Y.S., Fang, J., Zong, Y.Q., Shang, Z.W., Wang H.: The record of mid-Holocene maximum landward marine transgression in the west coast of Bohai Bay, China. Marine Geology, 359, 89–95. DOI: 10.1016/j.margeo.2014.11.013, 2015.

https://doi.org/10.5194/esurf-2020-21
Preprint. Discussion started: 16 April 2020

Earth Surface Dynamics
Discussions

Wang, H., Jia L., Wu P. Jiang, L., Hu, B. Xiang, L.: Effects of last-deglaciation on the historical relative sea levels of East Asia Seas and the implications. Chinese Journal of Geophysics, 55(4), 1144−1153. DOI: 10.6038/j.issn.0001-5733.2012.04.010, 2012.

Wang, H.: Chronology of Holocene chenier and oyster reefs on the coast of Bohai Bay, China. Quaternary Research, 47, 192−205. DOI: 10.1006/qres.1996.1865, 1997.

Wang, H., Chen, Y.S., Tian, L.Z., Li, J.F., Pei, Y.D., Wang, F., Shang, Z.W., Fan, C.F., Jiang, X.Y., Su, S.W., Wang, H.: Holocene cheniers and oyster reefs in Bohai Bay: palaeoclimate and sea level changes. Geological Bulletin of China, 30(9), 1405−1411. DOI: 10.1007/s11589-011-0776-4, 2011(in Chinese with English abstract).

Wang, H., Fan, C.F., Li, J.F., Li, F.L., Yan, Y.Z., Wang, Y.S., Zhang, J.Q., Zhang, YF.: Holocene oyster reefs on the northwest coast of the Bohai Bay, China. Geological bulletin of China, 25(3), 315−331. http://dzhtb.cgs.cn/gbc/ch/reader/create_pdf.aspx?file_no=20060354&flag=1&year_id=2006&quarter_id=3, 2006 (in Chinese with English abstract).

Wang, P.X., Min, Q.B. and Bian, Y.H.: Distributions of foraminifera and ostracoda in bottom sediments of the northwestern part of the South Huanghai (Yellow) Sea and its geological significance. In: Wang, P. (Eds.), Marine Micropaleontology of China. China Ocean Press, Beijing, pp. 93−114, 1985 (in Chinese with English abstract).

Wang, P.X., Min, Q.B., Bian, Y.H., Cheng, X.R.: Strata of quaternary transgressions in east China: a preliminary study. Acta Geologica Sinica, 1, 1−13. DOI: 10.1007/BF01077538, 1981 (in Chinese with English abstract).

Wang, R.B., Zhou, W., Li, F.L., Wang, H., Yang, G.Y., Yao, Z.J., Kuang, S.J.: Tectonic subsidence and prospect of ground subsidence control in Tianjin area. Hydrogeology & Engineering Geology, 5, 12-17. DOI: 10.1007/BF02873153, 2003 (in Chinese with English abstract).

Wang, Y.: The shell coast ridges and the old coastlines of the west coast of the Bohai Bay. Bulletin of Nanjing University (Edition of Natural Sciences), 8(3), 424−440. DOI: CNKI:SUN:NJDZ.0.1964-03-007, 1964 (with three plates) (in Chinese with English abstract).

Wang, Y.M.: A preliminary study on the Holocene transgression on the coastal plain along the north-western Bohai Bay. Geographical Research, 1(2), 59−69. DOI: 10.11821/yj1982020007, 1982 (in Chinese with English abstract).

Wang, Z., Zhuang, C., Staito, Y., Chen, J., Zhan, Q., Wang, X.: Early mid-Holocene sea-level change and coastal environmental response on the southern Yangtze delta plain, China: implications for the rise of Neolithic culture. Quaternary Science Reviews, 35, 51−62. DOI: 10.1016/j.quascirev.2012.01.005, 2012.

Wang, Z., Jones, B.G., Chen, T., Zhao, B., Zhan, Q.: A raised OIS3 sea level recorded in coastal sediments, southern Changjiang delta plain, China. Quaternary Research, 79, 424−438. DOI: 10.1016/j.yqres.2013.03.002, 2013.

Xiong, H., Zong, Y., Qian, P., Huang, G., Fu, S.: Holocene sea-level history of the northern coast of South China Sea. Quaternary Science Reviews 194, 12-26. https://doi.org/10.1016/j.quascirev.2018.06.022, 2018.

Xu, J.S.: Cheniers and sea level changes in Huanghua coast, Bohai Bay. Marine Science Bulletins, 1, 62−72. http://www.hyxb.org.cn/aos/ch/reader/create_pdf.aspx?file_no=19940109&flag=&journal_id=aos&year_id=1994, 1994 (in Chinese with English abstract).

Yang, H.R. and Chen, Q.X.: Quaternary transgressions, eustatic changes and shifting of shoreline in east China. Marine Geology & Quaternary Geology, 5(4), 69−80. DOI：10.16562/j.cnki.0256-1492.1985.04.011, 1985 (in Chinese with English abstract).

Zhang, Y.C., Hu, J.J. and Liu, C.F.: Preliminary recognition of sea and land changes along the east coast of China since the terminal Pleistocene. Bulletin of the Chinese Academy of Geological Sciences, 19, 37−52. https://www.ixueshu.com/document/8e1a59a8c6fd86ca318947a18e7f9386.html, 1989 (in Chinese with English abstract).

Zhao, S.L., Yang, G.F., Cang, S.X., Zhang, H.C., Huang, Q.F., Xia, D.X., Wang, Y.J., Liu, F.S., Liu, C.F.: On the marine stratigraphy and coastlines of the western coast of the gulf of Bohai. Oceanologia Et Limnologia Sinica, 9(1), 15−25. http://qdhys.ijournal.cn/hyyhz/ch/reader/create_pdf.aspx?file_no=19780102&flag=&journal_id=hyyhz&year_id=1978, 1978 (in Chinese with English abstract).

https://doi.org/10.5194/esurf-2020-21
Preprint. Discussion started: 16 April 2020

Earth Surface Dynamics Discussions Open Access

Zhao, X.T. (Eds.): The Holocene coastline shifts along the western coast of the Bohai Bay [M]//Institute of Geology, Academy of Sciences, Institute of Geology, State Bureau of Seismology. Formation and Development of the North China Fault Block Region. Beijing: Science Press, 302−309, 1980 (in Chinese).

Zong, Y.: Mid-Holocene sea-level highstand along the Southeast Coast of China. Quaternary International, 117(1), 55−67. DOI: 10.1016/S1040-6182(03)00116-2, 2004.

Zong, Y., Huang, G., Switzer, A.D., Yu, F., Yim, W.W.-S.: An evolutionary model for the Holocene formation of the Pearl River delta, China. The Holocene, 19, 129−142. DOI: 10.1177/0959683608098957, 2009.

Zong, Y., Huang, K., Yu, F., Zheng, Z., Switzer, A.D., Huang, G., Wang, N., Tang, M.: The role of sea-level rise, monsoonal discharge and the palaeo-landscape in the early Holocene evolution of the Pearl River delta, southern China. Quaternary Science Reviews, 54, 77−88. DOI: 10.1016/j.quascirev.2012.01.002, 2012.

https://doi.org/10.5194/esurf-2020-21
Preprint. Discussion started: 16 April 2020

Earth Surface Dynamics Discussions Open Access

Table 1. Analytical data used to establish SLIPs.

Beta-lab code	Depth (m)	Altitude (m, msl)	Dated material	$\delta^{13}C$ (‰)	Conventional age (BP)	Calibrated age (BP) (2σ)	Median age (BP)	Indicative meaning and range	Sediment compaction (m)*	Palaeo-mean sea level
Core DC01										
329636	8.40	-4.66	Peat	-26.8	6950±40	7523-7430	7487	Terrestrial peat		
329637	9.27	-5.53	Bulk organic	-18.2	7410±60	8372-8153	8248	Terrestrial peat		
Core QX01										
329647	5.52	+0.36	Bulk organic	-22.5	4300±30	4892-4829	4343**	1.78±0.53	0.29±0.04	-1.14±0.57
329644	6.35	-1.19	Bulk organic	-23.6	5010±50	5900-5644	5226**	1.78±0.53	0.30±0.04	-2.68±0.57
329643	7.20	-2.04	Bulk organic	-25.0	5090±30	5912-5748	5288**	1.78±0.53	0.25±0.03	-3.58±0.56
329641	8.20	-3.04	Peat	-24.6	5830±30	6732-6554	6647	1.78±0.53	0.24±0.03	-4.58±0.56
329642	8.70	-3.54	Peat	-24.3	6030±40	6981-6778	6875	1.78±0.53	0.21±0.03	-5.11±0.56
329645	9.16	-4.00	Peat	-27.4	6220±40	7250-7006	7117	1.78±0.53	0.18±0.02	-5.60±0.55
329640	11.39	-6.23	Peat	-25.3	7010±30	7935-7786	7855	1.78±0.53	0.01±0.01	-8.00±0.54
329646	13.05	-7.89	Peat	-25.1	7200±30	8057-7952	8002	Terrestrial peat		
Core QX03										
353792	2.91	1.47	Peat	-20.6	2350±30	2461-2326	2357	Terrestrial peat		
353794	4.90	-0.42	Peat	-24.0	3390±30	3699-3569	3634	1.78±0.53	0.16±0.02	-2.01±0.55
353796	7.39	-3.01	Plant material	NA	5930±30	6799-6671	6752	1.78±0.53	0.10±0.02	-4.68±0.55
353798	8.63	-4.25	Plant material	-26.7	6410±40	7420-7271	7350	1.78±0.53	0.01±0.01	-6.02±0.54
353800	9.60	-5.22	Plant material	-28.2	6690±40	7622-7478	7562	Terrestrial peat		
353802	12.40	-8.02	Plant material	-28.3	7280±40	8429-8325	8397	Terrestrial peat		
Core QX02										

https://doi.org/10.5194/esurf-2020-21
Preprint. Discussion started: 16 April 2020

Earth Surface Dynamics Discussions Open Access

332798	3.65	-0.08	Bulk organic	-23.6	3680±30	4091-3913	3517**	1.78±0.53	0.30±0.04	-1.57±0.57
332792	5.68	-2.11	Bulk organic	-24.0	5450±30	6300-6204	5718**	1.78±0.53	0.36±0.04	-3.54±0.57
333329	7.27	-3.70	Peat	-26.7	6350±30	7331-7240	7283	1.78±0.53	0.32±0.04	-5.16±0.57
333330	8.98	-5.41	Peat	-26.3	6600±30	7522-7434	7494	1.78±0.53	0.19±0.02	-7.00±0.55
333331	10.97	-7.40	Peat	-27.2	7020±30	7934-7792	7867	Terrestrial peat		
333333	12.42	-8.85	Peat	-26.3	7140±40	8023-7925	7966	Terrestrial peat		
Core ZW15										
255821	1.6	0.03	Bulk organic	-22.5	2930±30	3168-2976	2584**	1.78±0.53	0.32±0.04	-1.44±0.57
356208	12.6	-10.97	Plant material	-25.0	7450±40	8358-8186	8271	1.78±0.53	0.00	-12.75±0.53
356209	13.5	-11.87	Plant material	-25.5	7640±40	8521-8381	8430	Terrestrial peat		
Core Q7										
358054	1.3	2.16	Bulk organic	-20.4	530±30	559-510	540	1.78±0.53	0.10±0.02	+0.49±0.55
357153	17.2	-13.74	Plant material	-28.0	7990±40	9005-8705	8868	1.78±0.53	0.16±0.02	-15.36±0.55
357157	18.85	-15.39	Bulk organic	-24.6	9140±40	10411-10226	9718**	1.78±0.53	0.00	-17.18±0.53
Core CZ01										
395014	15.42	-8.53	Peat	-27.5	8930±40	10099-9914	10047	Terrestrial peat		
Core CZ02										
395022	12.19	-6.42	Peat	-23.1	7950±30	8980-8648	8830	Terrestrial peat		
Core CZ03										
395026	4.42	-0.48	Bulk organic	-24.2	2730±30	2877-2762	2325**	1.78±0.53	0.12±0.02	-2.15±0.55
395027	6.15	-2.21	Peat	-25.1	4790±30	5593-5470	5517	1.78±0.53	0.19±0.02	-3.80±0.55
395028	6.54	-2.57	Bulk organic	-27.1	5830±30	6732-6554	6114**	1.78±0.53	0.18±0.03	-4.18±0.56
395029	7.51	-3.54	Peat	-26.7	6230±30	7251-7019	7167	1.78±0.53	0.14±0.02	-5.19±0.55
395030	9.22	-5.25	Peat	-27.3	6640±30	7576-7468	7528	1.78±0.53	0.01±0.01	-7.03±0.54

https://doi.org/10.5194/esurf-2020-21
Preprint. Discussion started: 16 April 2020

Earth Surface Dynamics Discussions Open Access EGU

395031	9.34	-5.37	Peat	-20.0	6660±30	7583-7483	7535	1.78±0.53	0.00	-7.15±0.53
395032	10.23	-6.26	Peat	-27.2	6900±30	7794-7669	7726	Terrestrial peat		
395034	12.4	-8.43	Peat	-27.2	7290±30	8171-8025	8102	Terrestrial peat		
Core CZ87										
403413	2.66	1.8	Bulk organic	-20.8	2420±30	2696-2351	2446	Terrestrial peat		
403414	4.51	-0.05	Bulk organic	-23.8	3330±30	3637-3477	3566	Terrestrial peat		
406826	5.75	-1.29	Bulk organic	-24.1	4020±30	4536-4420	3970**	1.78±0.53	0.25±0.03	-2.83±0.56
403417	11.05	-6.59	Plant material	-27.9	6300±30	7275-7165	7223	1.78±0.53	0.04±0.01	-8.33±0.54
403418	12.62	-8.16	Plant material	-27.6	6990±30	7876-7736	7829	Terrestrial peat		
Core CZ61										
407339	2.52	1.24	Bulk organic	-20.8	2310±30	2359-2306	2337	Terrestrial peat		
406823	4.72	-0.96	Plant material	NA	2780±30	2952-2793	2877	1.78±0.53	0.16±0.02	-2.58±0.55
406824	6.20	-2.44	Bulk organic	-23.9	6100±30	7029-6884	6433**	1.78±0.53	0.25±0.03	-3.98±0.56
403397	9.73	-5.97	Plant material	-19.6	6760±30	7664-7577	7615	1.78±0.53	0.00	-7.75±0.53
403398	11.04	-7.37	Plant material	-27.5	7000±30	7932-7756	7842	Terrestrial peat		
403399	12.90	-9.14	Plant material	-28.0	7160±30	8018-7939	7980	Terrestrial peat		
Core CZ65										
399705	4.93	-1.97	Bulk organic	-18.5	3920±30	4428-4280	3397	Terrestrial peat		
399708	9.58	-6.62	Plant material	-27.2	7000±30	7883-7756	7823	1.78±0.53	0.01±0.01	-8.39±0.54
399710	11.50	-8.54	Plant material	-27.1	7250±30	8162-8001	8080	Terrestrial peat		
Core CZ80										
403401	3.73	2.69	Bulk organic	-20.3	3170±30	3452-3346	3400	Terrestrial peat		
403403	6.57	-0.15	Bulk organic	-22.1	5050±30	5901-5726	5298	1.78±0.53	0.20±0.03	-1.74±0.56
406825	8.75	-2.33	Peat	NA	5840±30	6736-6562	6660	1.78±0.53	0.09±0.01	-4.02±0.54

https://doi.org/10.5194/esurf-2020-21
Preprint. Discussion started: 16 April 2020

403408	11.53	-5.11	Plant material	-27.5	6450±30	7428-7313	7370	Terrestrial peat		
403409	12.05	-5.63	Plant material	-27.9	6610±30	7565-7440	7503	Terrestrial peat		
403410	12.34	-5.92	Plant material	-26.4	6860±30	7759-7618	7687	Terrestrial peat		
403411	13.84	-7.42	Plant material	-24.6	7300±30	8175-8029	8105	Terrestrial peat		
Core CZ85										
399719	3.67	0.94	Bulk organic	-20.5	3460±30	3671-3641	3225**	1.78±0.53	0.17±0.03	-0.68±0.56
399720	6.77	-2.16	Bulk organic	-25.4	5830±30	6732-6554	6114**	1.78±0.53	0.08±0.01	-3.87±0.54
399721	8.33	-3.72	Plant material	-26.4	6020±30	6947-6785	6862	1.78±0.53	0.01±0.01	-5.49±0.54
399722	12.70	-8.09	Plant material	-28.0	7270±30	8165-8015	8096	Terrestrial peat		
Core CZ66										
399712	3.62	0.25	Bulk organic	-23.4	3930±30	4440-4282	3856**	1.78±0.53	0.32±0.04	-1.22±0.57
399713	5.21	-1.34	Bulk organic	-25.1	5730±30	6632-6445	5992**	1.78±0.53	0.39±0.05	-2.74±0.58
399714	8.14	-4.27	Plant material	-27.4	6710±30	7651-7510	7581	1.78±0.53	0.24±0.03	-5.81±0.56
399715	10.03	-6.16	Plant material	-26.6	6790±30	7675-7587	7635	1.78±0.53	0.08±0.01	-7.86±0.54
399716	12.49	-8.62	Plant material	-27.1	7220±30	8156-7965	8021	Terrestrial peat		
399718	13.63	-9.76	Plant material	-27.6	7670±30	8523-8406	8452	Terrestrial peat		

s* Sediment compaction = 10% of compressible thickness divided by lapse time of deposition in the past 9000 years

** corrected for marine influence on salt marsh organic sample fraction ages of peaty clay

https://doi.org/10.5194/esurf-2020-21
Preprint. Discussion started: 16 April 2020

Earth Surface Dynamics Discussions

Figure captions

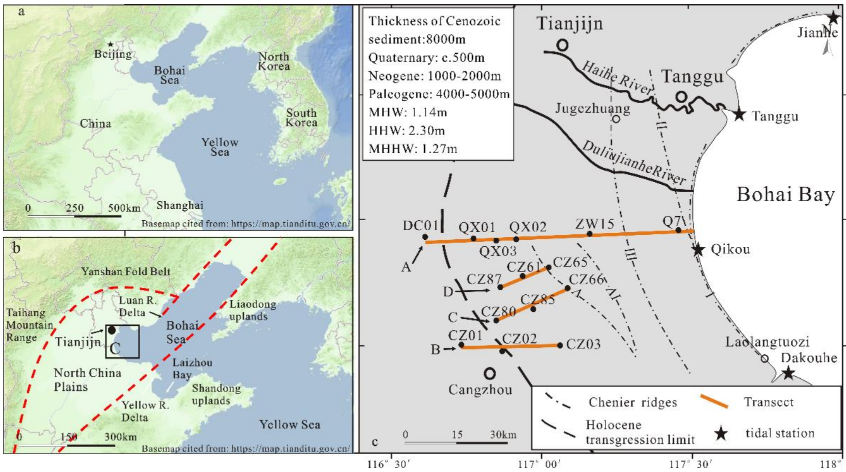

Figure 1. The study area; (a) location of Bohai Bay and Yellow Sea; (b) location of the study area and major river deltas; red dashed lines indicate the topographic boundaries of coastal lowland, (c) locations of boreholes, transects A, B, C, D, Chenier ridges (Su et al. (2011; Wang et al., 2011) and Holocene transgression limit (Xue, 1993). The basemap of Fig.1a and Fig.1b are cited from "map world" (https://www.tianditu.gov.cn/, National Plateform for Common Geispatial Information Services, China)

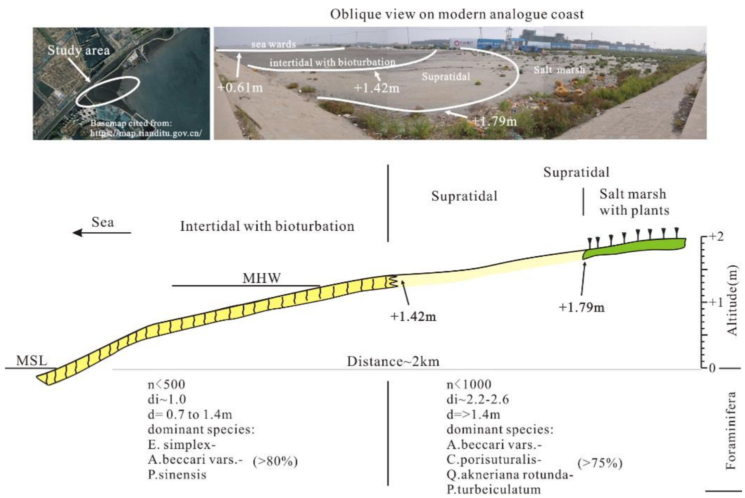

Figure 2. Schematic cross-section of the modern tidal flat of the study area showing two characteristic foraminiferal zones. The basemap of study area is cited from "map world" (https://www.tianditu.gov.cn/, National Plateform for Common Geispatial Information Services, China)

https://doi.org/10.5194/esurf-2020-21
Preprint. Discussion started: 16 April 2020

Earth Surface Dynamics Discussions
Open Access
EGU

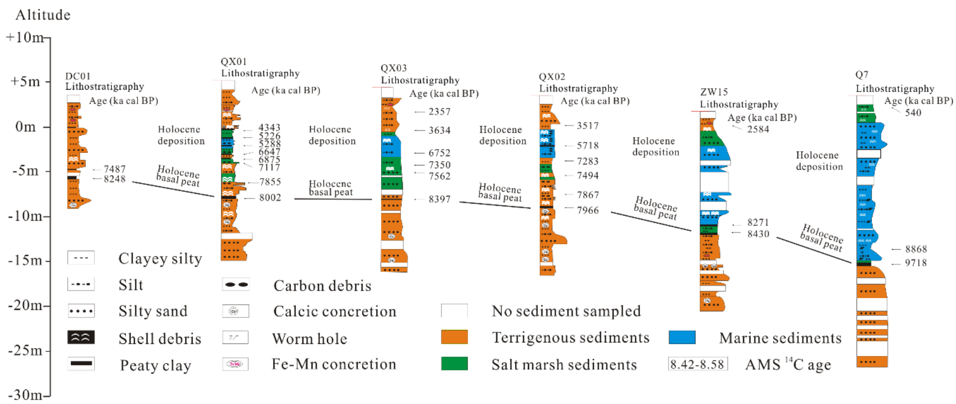

Figure 3. The lithostratigraphy of transect A, with details of dated sedimentary horizons.

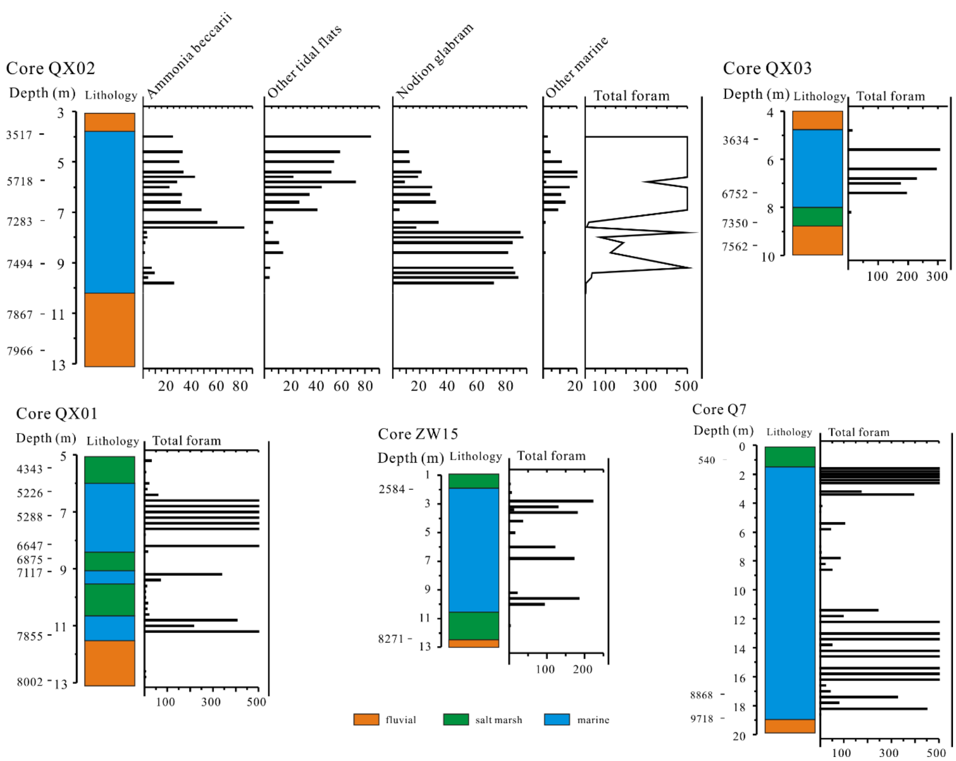

Figure 4. Foraminiferal counts from five cores of transect A. Counts > 500 are shown as 500.

498
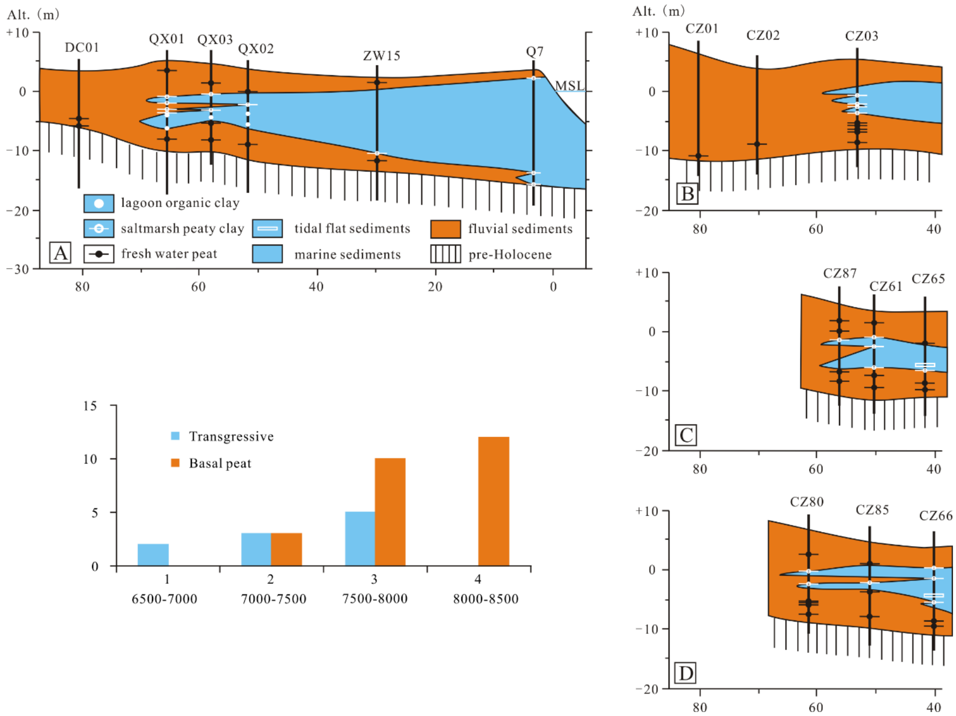

499 **Figure 5. The lithostratigraphy of transects B, C and D, with details of dated sedimentary horizons.**

https://doi.org/10.5194/esurf-2020-21
Preprint. Discussion started: 16 April 2020

Earth Surface Dynamics
Discussions
Open Access
EGU

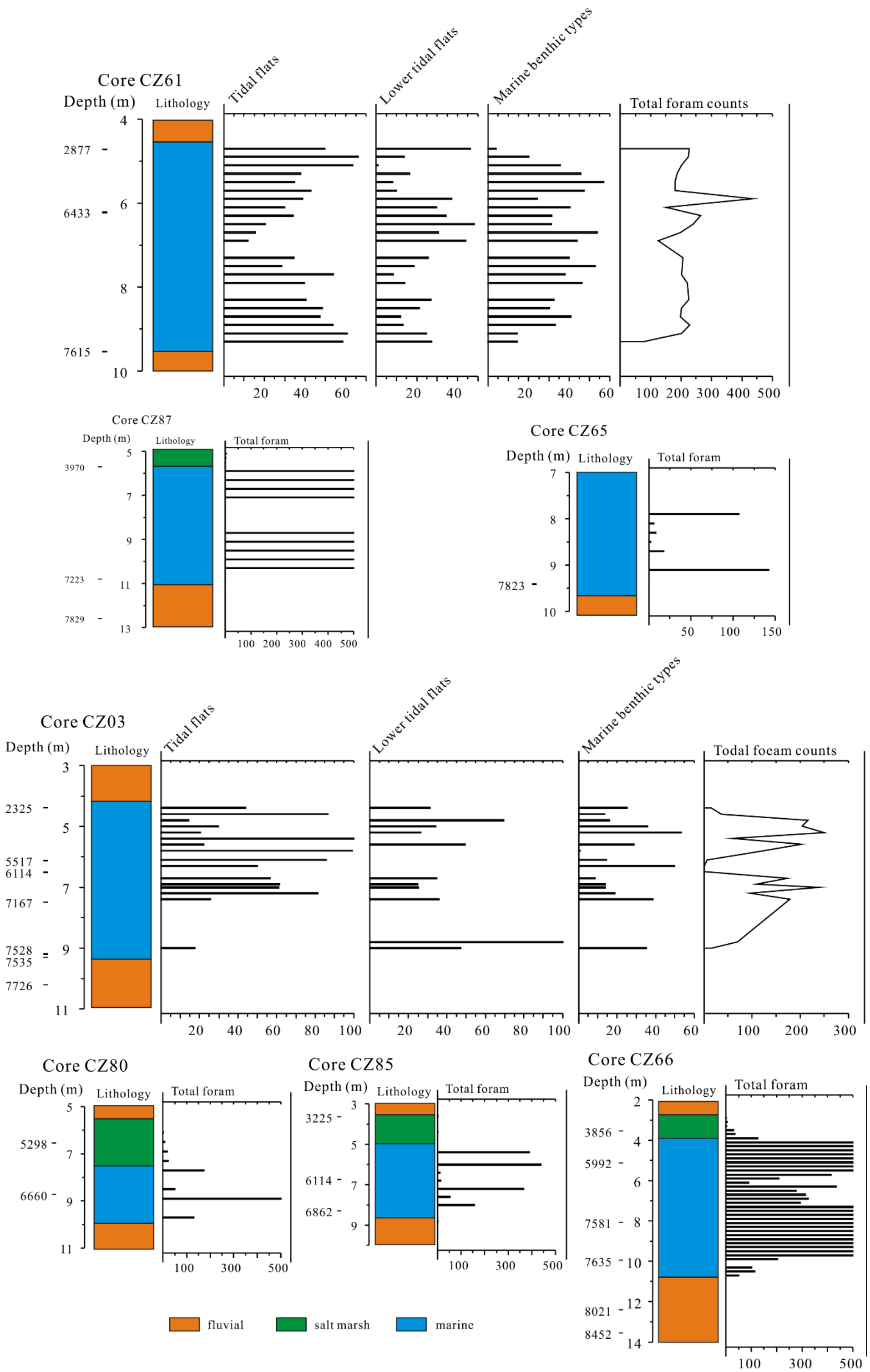

Figure 6. Foraminiferal counts from five cores of transects B, C and D. Counts > 500 foraminifera are shown as 500.

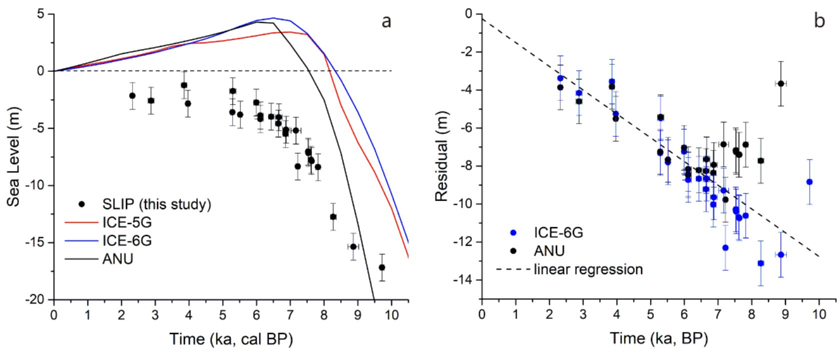

Figure 7. Observed and predicted sea level in Bohai Bay; (a) SLIPs generated in this study and sea-level predictions. ICE-5G, ICE-6G and ANU are ice models described in section 3.6. For model parameters see Table S1; (b) Sea-level residuals plotted against time. Residuals are the difference between SLIPs and interpolated model data points. Error bars are derived from SLIP uncertainties. The trend line (dashed line) is computed as a least-squares regression on the mean residuals obtained with ANU and ICE-6G. The regression line approximates zero elevation remarkably closely which gives confidence that the calculated 1.25 mm/a for the non-GIA component is correct.

https://doi.org/10.5194/esurf-2020-21
Preprint. Discussion started: 16 April 2020

Author contribution

Author name	Contributions
Fu Wang	Scientific questions choice, location choice of the boreholes, sampling, measuring, data analyse, results and discussion, entire paper writing.
Yongqiang Zong	Revise the part of of the paper and English writing.
Barbara Mauz	Revise the part of the paper and English writing.
Jianfen Li	Sampling and foraminifera analyse.
Jing Fang	Sampling and foraminifera analyse.
Lizhu Tian	Sampling and foraminifera analyse.
Yongsheng Chen	Sampling and foraminifera analyse.
Zhiwen Shang	Sampling and foraminifera analyse.
Xingyu Jiang	Sampling and foraminifera analyse.
Giorgio Spada	Modelling sea level part “3.6” and “5.3”
Daniele Melini	Modelling sea level part “3.6” and “5.3”